# Improving large-telescope speckle imaging via aperture partitioning

**Brandoch Calef**
*Boeing LTS Maui, 535 Lipoa Parkway Ste. 200, Kihei HI 96753*
**Eric Therkildsen**
*Boeing LTS Maui, 535 Lipoa Parkway Ste. 200, Kihei HI 96753*

## ABSTRACT

We describe a generalization of aperture masking interferometry that improves the speckle imaging performance of a telescope in the large $D/r_0$ regime while making use of all collected photons. Our approach is to partition the aperture into annuli, form the bispectra of the focal plane images formed from each annulus, recombine them into a synthesized bispectrum, and use that to retrieve the object. This may be implemented using multiple cameras and special mirrors, or with a single camera and a suitable pupil phase mask.

## 1. INTRODUCTION

When images are collected through the atmosphere, they are distorted due to refractive index fluctuations along the turbulent path [1]. The object may be recovered by the bispectrum technique, which exploits phase closure and atmospheric statistics to provide an estimate of the object's Fourier phase. As the ratio $D/r_0$ of the telescope aperture diameter to the atmospheric seeing cell size increases, the optical transfer function (OTF) is attenuated and the number of redundant baselines in the pupil increases, driving down the SNR of the bispectrum estimate.

The usual way of overcoming the latter degradation (which is sometimes called "baseline redundancy noise") is to collect short exposure images for many atmospheric decorrelation times. Averaging together their bispectra increases the SNR of the object bispectrum estimate in proportion to the square root of the number of independent atmospheric realizations. However, this approach is not always practical. For example, suppose that the subject of observation is a satellite passing overhead. Every few seconds, its orientation relative to the observer changes by an amount that is significant at the resolution of the telescope. This puts a limit on the time interval of frames that can be safely co-processed.

Another way of defeating redundancy noise is to mask the aperture, either with a pattern of holes whose diameters are on the order of $r_0$ (a non-redundant mask) or with a thin annulus at the outer edge of the pupil (a partially redundant mask). This approach is called aperture masking interferometry [2]. It eliminates or greatly reduces baseline redundancy noise at the expense of a much lower signal. This means that it can only be applied when the object is bright or when frames can be collected over a long period of time to accumulate signal.

We propose to extend this technique by partitioning the pupil and measuring the speckle patterns associated with each section. In this way, the redundancy noise is reduced while still making use of all light incident on the aperture. The natural partition is a set of concentric annuli, but it may be that another scheme is easier to implement. The only real constraint is that, taken together, the segments must provide spatial frequency coverage up to the diffraction limit. In the case of an annular partition, the outermost ring provides information at the highest spatial frequencies.

## 2. BISPECTRUM RECONSTRUCTION

### 2.1 Review of bispectrum technique

The object will be reconstructed from speckle images using the bispectrum, which we now review. Let $i(x)$ be a speckle image (focal-plane intensity pattern) formed by convolving an object $o(x)$ with an atmospheric point-spread function (PSF) $h(x)$. In Fourier space, this is written $I(u) = O(u)H(u)$. The bispectrum of $i(x)$ is defined by $B_I(u,v) = I(u)I(v)I^*(u+v)$, where $u$ and $v$ are both spatial frequencies. The bispectra of the object, PSF, and speckle image are therefore related by $B_I(u,v) = B_O(u,v)B_H(u,v)$. It can be shown that the expected bispectrum $\langle B_H(u,v)\rangle$ of the atmospheric PSF is strictly real (this will be discussed below), so the ensemble average speckle bispectrum has the same phase as the object bispectrum. From the bispectrum phase, the object's Fourier phase may be recovered up to an overall linear phase, which corresponds to a translation of the reconstructed image.

To implement this approach, a sequence of speckle images is collected and an estimate formed of the bispectrum of each one. In the presence of noise, an unbiased estimator of the bispectrum is given by

$$\hat{B}_I(u,v) = I(u)I(v)I^*(u+v) - |I(u)|^2 - |I(v)|^2 - |I(u+v)|^2 + 2K + 3n_{\text{pix}}\sigma^2, \tag{1}$$

where $K$ is the number of photoelectrons, $n_{\text{pix}}$ is the number of pixels, and $\sigma^2$ is the read noise variance in each pixel in photoelectrons. The bispectra of the individual frames are averaged together to form an ensemble estimate.

To see how the object may be recovered, consider the relationship between its Fourier phase and the bispectrum, given by $\arg B_O(u,v) = \arg O(u) + \arg O(v) - \arg O(u+v)$. Thus if the phase is known at $u$ and $v$, it may be recovered at $u+v$ by

$$\arg O(u+v) = \arg O(u) + \arg O(v) - \arg B_O(u,v). \tag{2}$$

To get this process started, observe that the dc term is always real, so $\arg O(0) = 0$. The choice of the first off-dc Fourier components governs the translation of the reconstructed image, which is arbitrary. From this point, repeatedly applying Eqn. 2 yields the entire phase map.

Having recovered the object's Fourier phase, one needs only the amplitude $|O(u)|$ to obtain a complete reconstruction. This may be achieved by making observations of a star under similar atmospheric conditions and using these to estimate the speckle transfer function $\langle |H|^2 \rangle$. Then

$$|O| = \left( \langle |I|^2 \rangle / \langle |H|^2 \rangle \right)^{1/2}. \tag{3}$$

### 2.2 Bispectrum estimation with a partitioned aperture

The effectiveness of the bispectrum technique hinges on the convergence of the bispectra of observed atmospheric PSFs to the purely real ensemble average. Taking the pupil amplitude to be unity and recalling that $H(u)$ is the autocorrelation of the pupil complex amplitude, the bispectrum of a wavefront with phase $\phi$ in the pupil is

$$\begin{aligned} B_H(u,v) = &\int_{P(0)\cap P(u)} \exp(i(\phi(w) - \phi(w+u)))\,dw \\ &\times \int_{P(0)\cap P(v)} \exp(i(\phi(w) - \phi(w+v)))\,dw \\ &\times \int_{P(0)\cap P(u+v)} \exp(i(\phi(w+u+w) - \phi(w)))\,dw, \end{aligned} \tag{4}$$

where $P(z)$ is the set of points in the pupil shifted by $z$. As the number of atmospheric cells in the pupil increases (due to increasing $D$ or decreasing $r_0$), the integral product yields a larger number of uncancelled phasor contributions to $B_H(u,v)$. This is the source of baseline redundancy noise.

Suppose that instead of a single full pupil, speckle images are collected simultaneously from several subregions of the aperture. If the aperture partition is constructed in such a way that the number of points in each region having a given vector separation is small, then the redundancy noise in the bispectrum estimate will be reduced.

Let $h_j(x)$ be the PSF associated with the $k$th subregion and let $i_j(x) = (h_j * o)(x)$ be the corresponding speckle image. To perform a bispectrum recovery from this information, form a bispectrum estimate $B_{I_k}(u,v)$ for each region. Then in the ensemble average, the phase of each region's bispectrum will match the object's bispectrum phase:

$$\arg \langle B_{I_k}(u,v) \rangle = \arg B_O(u,v). \tag{5}$$

Note that in general, each region will have a different diffraction cutoff, so for some $k$ the phase on the left-hand side of Eqn. 5 could be undefined for some $u$ and $v$.

A simple way of combining the bispectra of the subregions into a single bispectrum estimate is to calculate the sample variance of the estimates and use that to form a weighted mean bispectrum. Let $\sigma_k^2(u,v)$ be the sample variance of $B_{I_k}(u,v)$. Then let

$$B_{\text{syn}}(u,v) = \sum_k \frac{B_{I_k}(u,v)}{\sigma_k(u,v)} \Bigg/ \sum_k \frac{1}{\sigma_k(u,v)} \tag{6}$$

be the synthesized bispectrum estimate. Note that this is weighting by standard deviation, not by variance as one might expect. In simulation results, the standard deviation was found to produce a better result.

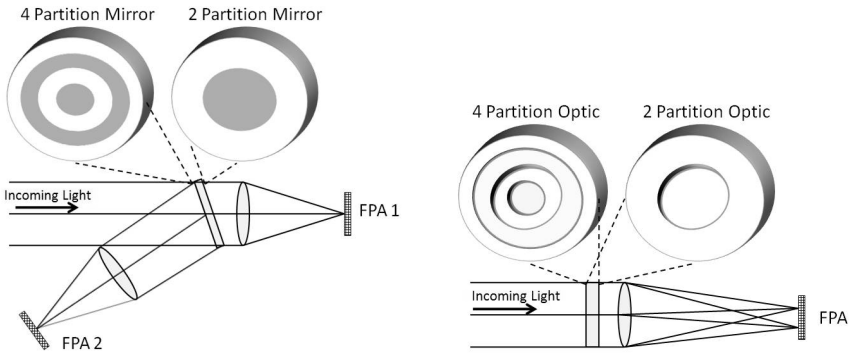


(a) (b)

Figure 1. Two possible implementations of aperture partitioning. (a) One or more mirrors split the pupil, sending the light from different subregions to be focused on different FPAs. (b) A pupil phase mask puts different tilts on the different subregions, causing the images to be focused on different parts of a single FPA.

## 3. DESIGN

Implementing aperture partitioning requires that the hardware be configured so that each part of the pupil forms its own image. One way of accomplishing this is illustrated in Fig. 1(a). A mirror placed at a pupil breaks up the beam. Each subregion is focused onto a separate focal-plane array (FPA) (only two in the figure). If the subregions are all annular, this could be accomplished using just flat mirrors with holes drilled in them. Note that since the bispectrum is shift-invariant, the alignment of the FPAs relative to boresight does not need to be perfect.

Another approach, illustrated in Fig. 1(b), is to use a single camera and introduce a pupil phase mask that puts different tilts on the different aperture subregions. This yields several speckle patterns offset from each other on the FPA. One way of reconstructing an image from this system is use a suitable window to pick out each speckle channel and process as before. An alternative is to use a multiframe blind deconvolution algorithm with the aperture-partitioning phase mask included in the forward model. This recovers the wavefronts as well as the object image.

## 4. SIMULATION AND RESULTS

### 4.1 Simulation description

To test the performance of this technique, we simulated a system with a 3.6 m aperture collecting data at 30 Hz in the I band. The atmosphere is modeled using the Maui-3 $C_n^2$ profile, scaled to yield various turbulence strengths. The atmosphere is broken into four slabs to capture the effects of slew and wind. The FPAs are $256 \times 256$ CCDs with sky foreground and photon noise modeled, but no read noise. Unless otherwise noted, the results shown are for an aperture partitioned into three concentric annuli, a sidereal slew rate, a ground wind speed of 4 m/s, and one second's worth of data (30 frames).

### 4.2 SNR results

For conventional full-aperture speckle imaging, various authors [3–5] have derived analytic approximations of the SNR of the bispectrum estimate. These calculations are based on the assumption that the aperture contains a large number of statistically independent atmospheric cells, which is approximately true in the mid-frequency region with a full aperture. However, this does not hold for the annular subapertures that are of interest here. Instead, we depend on simulations to provide measurements of the bispectrum SNR.

Fig. 2 shows the bispectrum SNR in the plane $u = (x, 0)$, $v = (0, y)$ when $D/r_0 = 16$. The left side is obtained from the full aperture. The right side is the result obtained via Eqn. 6 from the partitioned aperture. On the left side, the usual features are visible [3]: very high SNR near the origin, high SNR along the $\|u\| \approx 0$ and $\|v\| \approx 0$ axes, and a plateau of much lower SNR out to the diffraction limit. The partitioned aperture has a similar structure, but the regions of high SNR extend further out from the axes. A "ring" structure is visible in the SNR map due to the annular partitions of the pupil.

In Fig. 3, the turbulence strength has been increased to give $D/r_0 = 40$. The color scale matches that of Fig. 2, so the SNR is clearly lower everywhere. As before, the partitioned aperture yields higher SNR, especially in the region off-axis

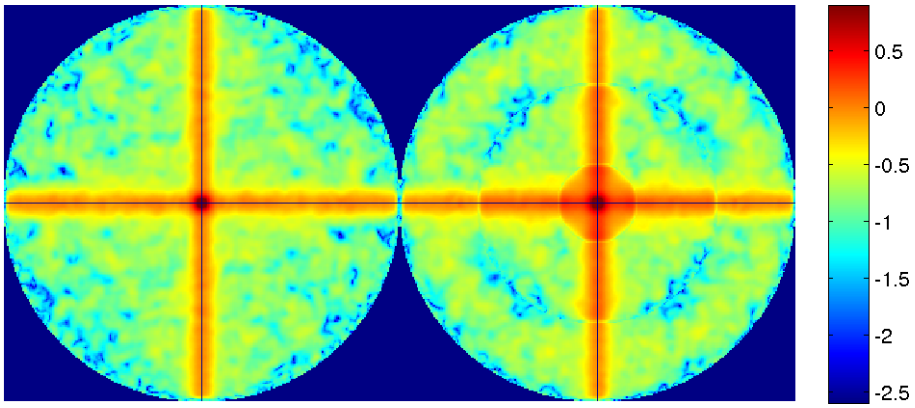


Full aperture Partitioned aperture

Figure 2. The logarithm (base 10) of the bispectrum SNR in the subplane $u = (x, 0)$, $v = (0, y)$. On the left, the bispectrum is formed from the full pupil. On the right, the bispectrum estimate is formed from an aperture divided into three concentric annuli. The $C_n^2$ profile was scaled to yield $D/r_0 = 16$.

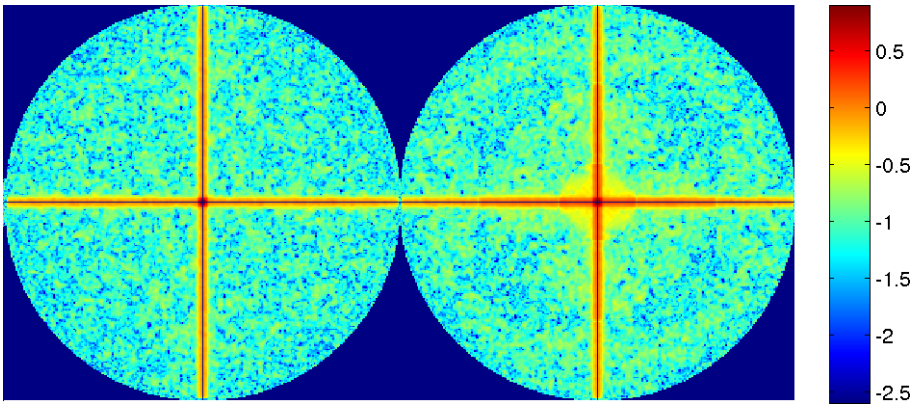


Full aperture Partitioned aperture

Figure 3. The bispectrum SNR for the full and partitioned aperture with $D/r_0 = 40$.

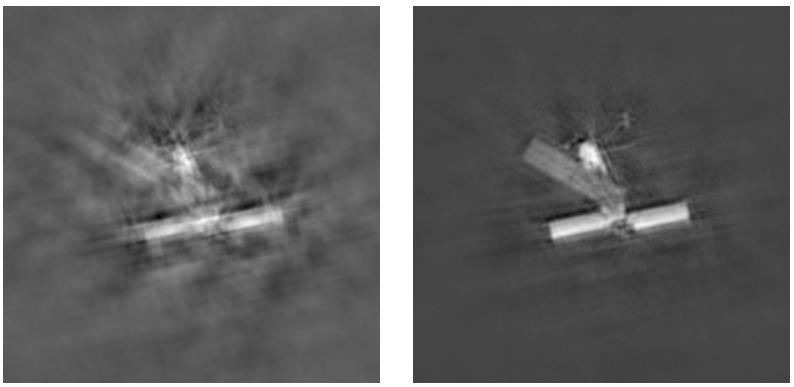

Full aperture Partitioned aperture

Figure 4. Reconstructed images from a full aperture (left) and partitioned aperture (right) with $D/r_0 = 64$ and sidereal slew rate. Both data sets were generated from the same simulated wavefronts. The target brightness was scaled to yield visual magnitude of 1, which gives a peak SNR of 820 on the full aperture FPA.

but close to the origin. The importance of this region to the quality of the object phase reconstruction is evident from Eqn. 2. If $B_O(u, v)$ is noisy when $\|u\| \neq 0$, $\|v\| \neq 0$, then the estimate of $O(u + v)$ obtained from $O(u)$ and $O(v)$ will also be noisy.

### 4.3 Image results

To get an idea of how the improved SNR translates into image quality, we now look at a series of comparisons between full-aperture and partitioned-aperture reconstructed images. In each case, the same wavefronts are used to generate the simulated images from which the reconstructions are formed.

Fig. 4 illustrates the case of $D/r_0 = 64$ for a bright (visual magnitude $m_v = 1$) target. Recall that partitioning the aperture both boosts the OTF and reduces the baseline redundancy noise. Boosting the OTF would result in less noise amplification in the higher spatial frequencies, but in this case the SNR is so high that there is virtually no sensor noise to amplify. On the other hand, there is a great deal of baseline redundancy noise, and by reducing it the partitioning method produces a much better result.

In Fig. 5, the target brightness is varied from 1st mag to 10th mag. In each case the partitioned aperture yields the superior result. This is somewhat counterintuitive, since splitting the aperture to form separate images means that each partitioned-aperture speckle image will have lower SNR than the full-aperture speckle images. However, under the conditions simulated here, this is not sufficient to outweigh the advantages of the partitioning technique. Presumably this would no longer be the case if the sensor read noise were sufficiently high.

As the turbulence strength increases (Fig. 6), the degree of baseline redundancy increases, causing the full-aperture images to suffer. Breaking up the pupil suppresses this source of error, greatly improving the reconstructed image quality.

Fig. 7 shows the effect of slew rate on image quality. As the slew rate increases, the phase in the pupil decorrelates more quickly. This improves the performance of the full-pupil results because redundancy noise can be effectively averaged out using independent realizations of the atmosphere. It has less effect on the partitioned-aperture setup, which enjoys a much lower level of redundancy noise.

Finally, we consider the effect of the changing the number of annuli into which the pupil is partitioned. As shown in Fig. 8, if there are too few annuli, then there is enough redundancy in each annulus to yield perceivable noise in the recovered image. However, as the number of annuli increases, the available light is split between more and more FPAs, reducing the SNR on each one. For the system modeled here, the best performance is obtained with 3 or 4 annuli.

## 5. CONCLUSIONS

We have described a technique for improving speckle imaging performance by partitioning the telescope aperture. In simulation results, we find that when $D/r_0 \gg 1$ and the slew rate is fairly low, it greatly outperforms conventional full-aperture imaging. Unlike aperture masking interferometry, this advantage is maintained even for dim targets.

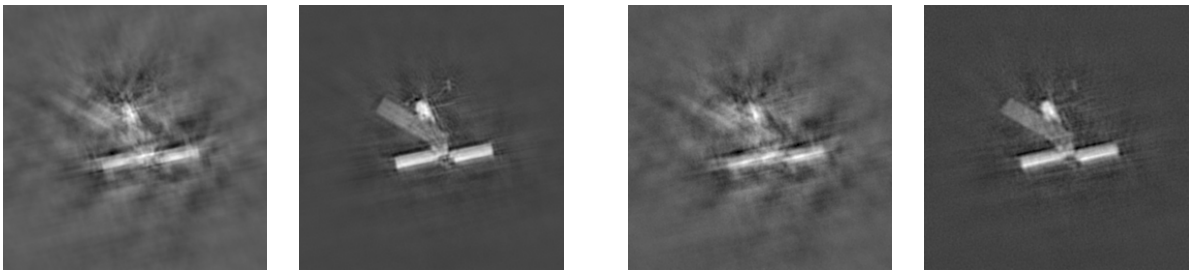

Full aperture Partitioned aperture Full aperture Partitioned aperture

$m_v = 1$ $m_v = 4$

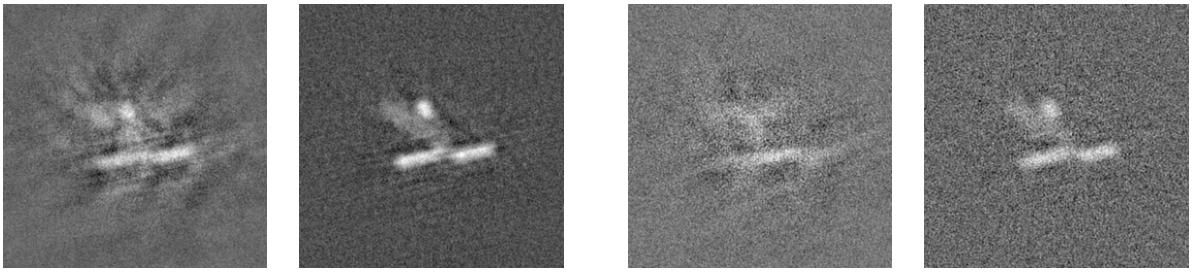

Full aperture Partitioned aperture Full aperture Partitioned aperture

$m_v = 8$ $m_v = 10$

Figure 5. Full aperture vs. partitioned aperture as a function of target brightness. The peak pixel SNR on the full aperture FPA varies from 13 at 10th mag to 820 at 1st mag.

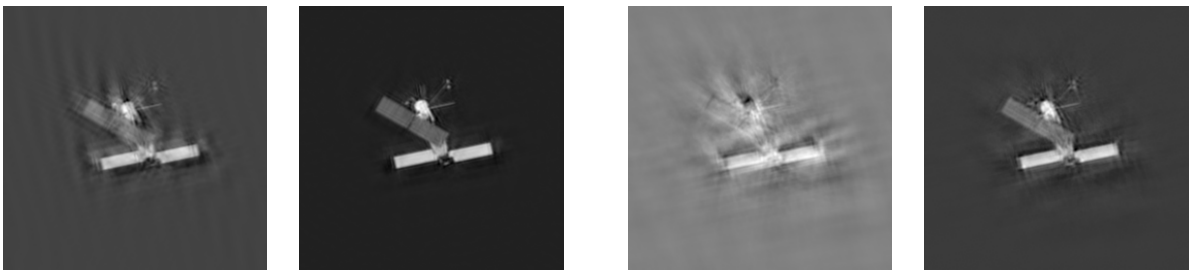

Full aperture Partitioned aperture Full aperture Partitioned aperture

$D/r_0 = 16$ $D/r_0 = 40$

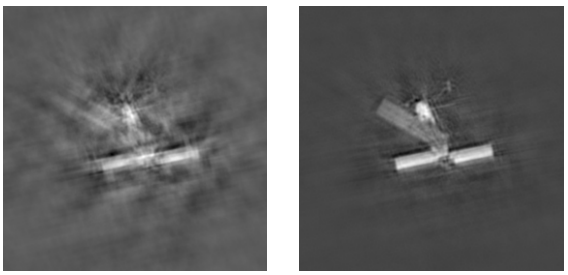

Full aperture Partitioned aperture

$D/r_0 = 64$

Figure 6. Full aperture vs. partitioned aperture as a function of turbulence strength. The increase in redundancy noise causes an obvious deterioration in the quality of the full-aperture results.

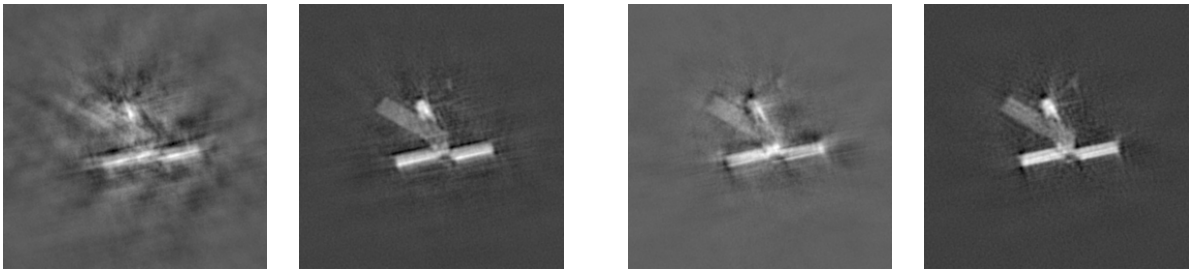

Full aperture Partitioned aperture Full aperture Partitioned aperture

Sidereal slew 0.02°/sec slew

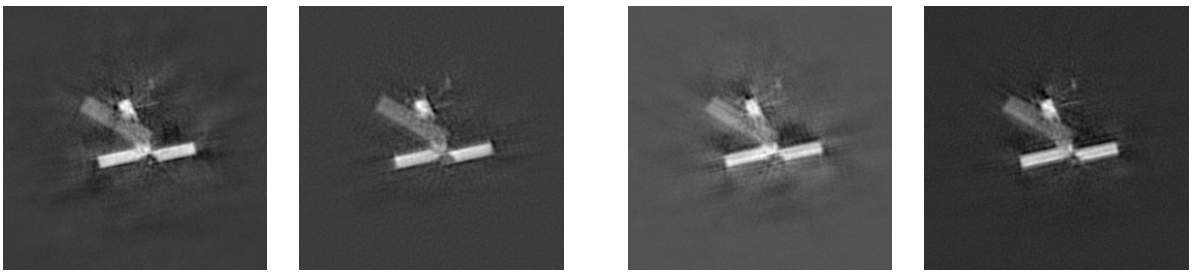

Full aperture Partitioned aperture Full aperture Partitioned aperture

0.2°/sec slew 0.5°/sec slew

Figure 7. Full aperture vs. partitioned aperture as a function of slew rate with $m_v = 4$. As slew rate increases, the measured atmospheric realizations become completely decorrelated, beating down redundancy noise.

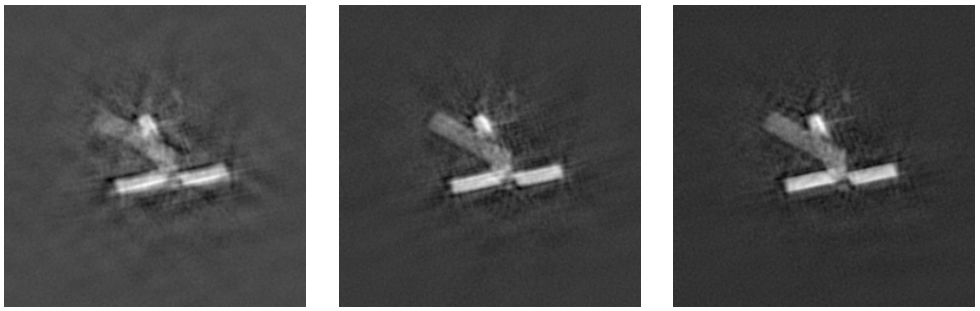

2 annuli 3 annuli 4 annuli

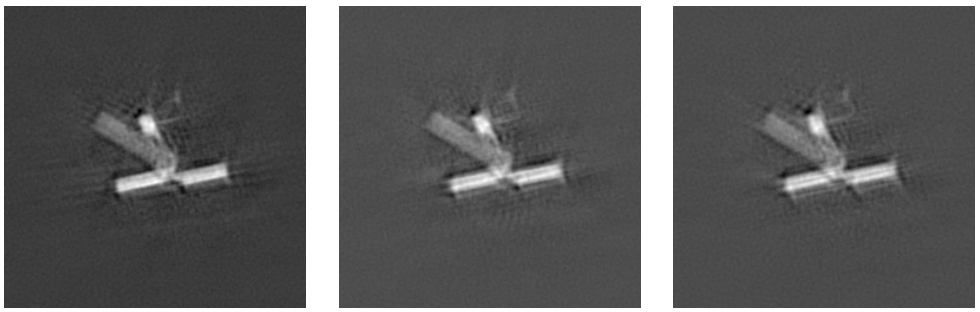

5 annuli 6 annuli 7 annuli

Figure 8. Partitioned-aperture results as a function of the number of annuli, with $D/r_0 = 64$ and $m_v = 4$. The trade-off between redundancy noise and signal level is apparent.

## ACKNOWLEDGMENTS

The authors thank Chuck Matson for his support and for relevant pointers in the literature. This work was funded by the Air Force Office of Scientific Research through AFRL contract FA9451-05-C-0257.

## REFERENCES

[1] Roggemann, M. C. and Welsh, B., *Imaging Through Turbulence*, CRC Press (1996).

[2] Haniff, C. A., Buscher, D. F., Christou, J. C., and Ridgway, S. T., "Synthetic aperture imaging at infrared wavelengths," *Monthly Notices of the Royal Astronomical Society* **241**, 51–56 (1989).

[3] Nakajima, T., "Signal-to-noise ratio of the bispectral analysis of speckle interferometry," *Journal of the Optical Society of America A* **5**(9), 1477–1491 (1988).

[4] Ayers, G. R., Northcott, M. J., and Dainty, J. C., "Knox-Thompson and triple-correlation imaging through atmospheric turbulence," *Journal of the Optical Society of America A* **5**(7), 963–985 (1988).

[5] Chelli, A., "The phase problem in optical interferometry: error analysis in the presence of photon noise," *Astronomy and Astrophysics* **225**, 277–290 (1989).